AIAA JOURNAL
Vol. 44, No. 11, November 2006

# Upstream Condition Effects on Turbulent Boundary Layers Subject to Favorable Pressure Gradients

Raúl Bayoán Cal*
*Rensselaer Polytechnic Institute, Troy, New York 12180*
Gunnar Johansson†
*Chalmers University of Technology, 412 96 Gothenburg, Sweden*
and
Luciano Castillo‡
*Rensselaer Polytechnic Institute, Troy, New York 12180*

DOI: 10.2514/1.19768

**The effects of the upstream conditions in favorable pressure gradient boundary layers are studied by carrying out an experiment using laser-doppler anemometry over multiple traverses along a smooth plate. A set of upstream conditions composed of upstream wind tunnel speed, tripwire location, and the strength of the pressure gradient is analyzed. The similarity analysis of the equations of motion for pressure gradient flows is used to obtain the scales for the outer flow. For this study, the mean deficit profiles show a small dependence on the strength of the pressure gradient when scaled with the freestream velocity $U_\infty$. Second, the upstream conditions effects are removed from the velocity deficit profiles when normalized by the $U_\infty \delta_*/\delta$ scaling. However, the Reynolds stress profiles show the effects of upstream conditions and the strength of the pressure gradient. Finally, these favorable pressure gradient flows are found to be nonequilibrium flows because the pressure parameter $\Lambda$ is not constant. In addition, three quadrants are found to describe all pressure gradient flows: one for adverse pressure gradient, one for favorable pressure gradient, and one for quasi-laminar flows, where different values are obtained and these are dependent on the experimental conditions. The quadrants are obtained by plotting $\log(U_\infty/U_{\infty i})$ versus $\log(\delta/\delta_i)$.**

## Nomenclature

| | | |
|---|---|---|
| $f_{\text{op}}$ | = | outer velocity profile (at finite $\delta^+$) |
| $f_{\text{op}_\infty}$ | = | asymptotic outer velocity profile in the limit as $\delta^+ \to \infty$ |
| $H$ | = | shape factor, $\frac{\delta_*}{\theta}$ |
| $K$ | = | acceleration parameter, $\frac{\nu}{U_\infty^2}\frac{dU_\infty}{dx}$ |
| $R_{\text{so}}$ | = | unknown outer Reynolds stress scale |
| $Re_{d_o}$ | = | Reynolds number based on the diameter of the tripping device |
| $Re_{x_o}$ | = | Reynolds number based on the position of the tripping device |
| $Re_\theta$ | = | Reynolds number based on the momentum thickness $\theta$ |
| $U_o$ | = | upstream wind-tunnel speed |
| $U_{\text{so}}$ | = | unknown outer velocity scale |
| $U_\infty$ | = | freestream velocity |
| $U_\infty - U$ | = | mean velocity deficit |
| $U_\infty(\delta_*/\delta)$ | = | velocity scaling |
| $\langle u^2 \rangle$ | = | Reynolds normal stress in the streamwise direction |
| $\langle uv \rangle$ | = | Reynolds shear stress |
| $\langle v^2 \rangle$ | = | Reynolds normal stress in the wall-normal direction |
| $\bar{y}$ | = | outer similarity length scale, $y/\delta_{95}$ or $y/\delta_{99}$ |
| $y^+$ | = | inner similarity length scale, $yu_*/\nu$ |
| $\alpha$ | = | angle of the plate |
| $\beta$ | = | pressure parameter, $(\delta_*/\rho u_*^2)(dP_\infty/dx)$ |
| $\delta$ | = | boundary layer thickness, e.g., $\delta_{95}$ |
| $\delta_*$ | = | displacement thickness, $\int_0^\infty (1 - \frac{U}{U_\infty})\,\mathrm{d}y$ |
| $\delta^+$ | = | local Reynolds number dependence, $\delta/\eta = \delta_{u_*}/\nu$ |
| $d\delta/dx$ | = | boundary layer growth rate |
| $\theta$ | = | momentum thickness, $\int_0^\infty \frac{U}{U_\infty}(1 - \frac{U}{U_\infty})\,\mathrm{d}y$ |
| $\Lambda$ | = | pressure parameter, $[\delta/(\rho U_\infty^2 d\delta/dx)](dP_\infty/dx) = -[\delta/(U_\infty d\delta/dx)](dU_\infty/dx)$ |
| * | = | unknown dependence on upstream conditions |

Presented as Paper 4812 at the 4th AIAA Theoretical Fluid Mechanics Meeting, Toronto, Ontario, 6–9 June 2005; received 30 August 2005; revision received 7 July 2006; accepted for publication 7 July 2006. 

*Ph.D. Graduate Student, Department of Mechanical, Aerospace, and Nuclear Engineering.
†Associate Professor, Department of Applied Mechanics.
‡Associate Professor, Department of Mechanical, Aerospace, and Nuclear Engineering; also Department of Mechanical Engineering, University of Puerto Rico–Mayagüez, Mayagüez, Puerto Rico, AIAA member.

## I. Introduction

THE favorable pressure gradient (FPG) turbulent boundary layer is of interest in the turbulence community because it is a fundamental problem that may be applied to different areas in industry. Moreover, it has become important to study the effects of upstream or influential external conditions on the flow as it develops downstream. In turn, these conditions may serve as a tool for flow control. In the past, it has been believed that the effects of upstream conditions disappear as the Reynolds number increases [1,2]. Upstream conditions may entail effects such as tripwire size, position, and geometry, as well as upstream wind-tunnel speed. This problem is studied by carrying out experiments on an inclined plate. Measurements of the velocity field are performed via laser-doppler anemometry (LDA) in a closed-loop wind-tunnel at Chalmers University of Technology. Furthermore, it is possible to observe the development of the turbulent boundary layer in a critical manner by normalizing both the velocity profiles and the Reynolds stress profiles in outer variables.

The scales for the velocity and Reynolds stresses were obtained for pressure gradient flows by Clauser [3] through dimensional analysis as proposed by von Kármán [4] and Millikan [5]. They proposed the friction velocity $u_*$ as a single velocity scale for turbulent boundary layers. This scaling was used in the experimental study of Erm and Joubert [6] for the velocity and Reynolds stress profiles on a zero pressure gradient (ZPG) flow. In this study, they used several tripping conditions to disturb the flow and concluded that these

devices (i.e., tripwire, distributed grit, and cylindrical pins) do not affect the velocity profiles. The same conclusions were drawn for the Reynolds stresses with the exception of the cylindrical pins. Recently, Castillo and Johansson [7] showed that the mean velocity deficit profiles were not affected by tripping devices, although they scaled the profiles using the freestream velocity. More important, they showed that the effects of the upstream conditions were observed on the Reynolds stresses for a zero pressure gradient boundary layer.

Experimentally, favorable pressure gradient boundary layer flows have been studied, but none have explored the specific issue of the effects of upstream conditions on the outer flow. In many of the most recent experiments [8–10], the problem classically termed as relaminarization is studied. Relaminarization occurs when a relatively strong favorable pressure gradient is imposed on the flow. The quantification of the acceleration due to the pressure gradient as well as the prediction of relaminarization have been traditionally performed using an acceleration parameter characterized by Launder [11] as

$$K = \frac{\nu}{U_\infty^2}\frac{dU_\infty}{dx}$$

However, Sreenivasan [12] concluded that this parameter was not sufficient to predict the relaminarization phenomenon. A benchmark experiment, performed by Ludwieg and Tillmann [13], was one of the first performed on FPG turbulent boundary layers. These data will be used for comparison in this study, however, details about the upstream conditions are not known for this experiment. Following the work of Ludwieg and Tillmann, numerous experiments were performed on FPG turbulent boundary layers. However, none of them carefully examined the effects of upstream conditions on the downstream flow. An experiment by Herring and Norbury [14] was performed on FPG turbulent boundary layers using two different strengths for the pressure gradient, although careful note of the upstream conditions and Reynolds stresses were not reported. The data were compared with zero and adverse pressure gradient (APG) experiments carried out by Clauser [3]. Furthermore, the velocity profiles were normalized with the friction velocity, which failed to collapse the profiles into a single curve.

Kline et al. [15] carried out measurements on various pressure gradient turbulent boundary layers including FPG flows. In their studies, they used the acceleration parameter $K$ to describe different pressure gradient flows where various water-tunnel geometry configurations were used. They also used visualization techniques of the boundary layer where the visual mean streak spacing was used to quantify the observed changes. Furthermore, formation and break-up of low-speed streaks were seen in their turbulent boundary layers studies. More interestingly, they showed that the viscous sublayer region collapsed as expected (i.e., $U^+ = y^+$). However, the overlap layer showed a dependence on the Reynolds number as well as on pressure gradient when normalized by the friction velocity obtained from the slope-at-the-wall method (velocity gradient). On the other hand, the overlap region collapsed, but the profiles in the viscous sublayer showed a Reynolds number dependence when normalized using the friction velocity obtained from the Clauser [3] method.

More recently, Fernholz and Warnack [16] performed an experiment using hot wire to measure the mean velocity as well as the turbulent quantities. Several techniques were employed to measure the skin friction (i.e., Preston tubes, surface fences, wall-hot wire, and oil film interferometry). They showed that the logarithmic law fails to properly describe the overlap region in many of their cases of FPG flows. A similar study was done by Ichimiya et al. [9], which used the variable-integral time averaging technique to observe the ejection and sweep behavior in the turbulence fluctuations. Higher order moments, time scales, and power spectra were also analyzed in their study.

A special kind of FPG flow is a sink flow, which has a pressure gradient with the geometry of a two-dimensional (2-D) potential sink. This flow is confined between a horizontal flat plate and a plate at an angle. Jones et al. [17] uniquely characterized a sink flow with the acceleration parameter $K_{\text{sink}}$ given by

$$K_{\text{sink}} = \frac{\nu}{U_o L} \tag{1}$$

which is a positive constant, where $\nu$ is the kinematic viscosity of the fluid and $L$ is the length of the measuring section. Furthermore, sink flows were studied with $K_{\text{sink}}$ values from $1.5 \times 10^{-6}$ to $5.39 \times 10^{-7}$ by Jones et al. [17] and it was concluded that equilibrium was approached when $(x/L) \sim 0.60$. This type of flow meets the requirements for an equilibrium flow as first described by Townsend [18] and later by Rotta [19]. According to their study, this flow is in equilibrium in the sense that the mean deficit velocity profiles and Reynolds stress profiles are invariant with the streamwise coordinate $x$ or Reynolds number. These equilibrium conditions were satisfied, but they were done under very specific conditions like the set of measurements performed by Skåre and Krogstad [20] subjected to an adverse pressure gradient. Moreover, Castillo and Johansson [7] showed that if the upstream conditions are fixed, the mean velocity and
Reynolds stresses are nearly independent of Reynolds number in ZPG flows.

Therefore, the goal of this investigation is to explore if the upstream conditions have an effect on the outer flow of the turbulent boundary layer by isolating specific upstream conditions. This study is performed by using the similarity analysis for pressure gradient proposed by Castillo and George [21] and LDA measurements.

### A. Similarity Analysis

Using the equations of motion and the accompanying boundary conditions, it is possible to obtain the scales for the flow without having to assume anything about the scales a priori by applying equilibrium similarity analysis. Details have been carried out in Castillo and George [21] for the pressure gradient turbulent boundary layer. After reaching the form of these different similarity solutions, the asymptotic invariance principle (AIP) can be employed [22]. The AIP states that in the limit as Reynolds number approaches infinity, the boundary layer equations for the outer flow become independent of the Reynolds number $\delta^+$ and in the same manner, the properly scaled solutions are also independent [22]. Therefore, the preceding similarity solutions should yield Reynolds number invariant solutions (but only in this limit) of the following form:

$$\frac{U_\infty - U}{U_{\text{so}}(x)} = f_{\text{op}}(\bar{y}, \delta^+, \Lambda, *) \to \lim_{\delta^+\to\infty} f_{\text{op}}(\bar{y}, \delta^+, \Lambda, *) = f_{\text{op}\infty}(\bar{y}, \Lambda, *) \tag{2}$$

$$\frac{-\langle uv\rangle}{R_{\text{so}_{uv}}(x)} = r_{\text{op}_{uv}}(\bar{y}, \delta^+, \Lambda, *) \to \lim_{\delta^+\to\infty} r_{\text{op}_{uv}}(\bar{y}, \delta^+, \Lambda, *) = r_{\text{op}\infty_{uv}}(\bar{y}, \Lambda, *) \tag{3}$$

$$\frac{\langle u^2\rangle}{R_{\text{so}_u}(x)} = r_{\text{op}_u}(\bar{y}, \delta^+, \Lambda, *) \to \lim_{\delta^+\to\infty} r_{\text{op}_u}(\bar{y}, \delta^+, \Lambda, *) = r_{\text{op}\infty_u}(\bar{y}, \Lambda, *) \tag{4}$$

$$\frac{\langle v^2\rangle}{R_{\text{so}_v}(x)} = r_{\text{op}_v}(\bar{y}, \delta^+, \Lambda, *) \to \lim_{\delta^+\to\infty} r_{\text{op}_v}(\bar{y}, \delta^+, \Lambda, *) = r_{\text{op}\infty_v}(\bar{y}, \Lambda, *) \tag{5}$$

The arguments inside the similarity functions $f_{\text{op}}$, $r_{\text{op}_{uv}}$, $r_{\text{op}_u}$, and $r_{\text{op}_v}$ are the outer similarity coordinate $\bar{y} = \frac{y}{\delta_{95}}$, the Reynolds number dependence $\delta^+ = \frac{\delta u_*}{\nu}$, the pressure parameter $\Lambda$, and the upstream conditions $*$, respectively. The unknown scalings for the different quantities are represented by $U_{\text{so}}$, $R_{\text{so}_{uv}}$, $R_{\text{so}_u}$, and $R_{\text{so}_v}$ (i.e., are only a function of $x$). In this particular problem, the influences of the last two parameters $(\Lambda, *)$ on each of the dependent variables is of

interest in this investigation. The parameter $*$ is specifically composed of quantities that come in as boundary conditions and are represented in the form of upstream Reynolds numbers (i.e., $Re_{x_o}$ and $Re_{d_o}$) as well as any other unknown dependence (for details refer to Johansson and Castillo [23]).

The similarity functions in the limit as Reynolds number approaches infinity are denoted with the subscript op$\infty$, meaning that they are independent of Reynolds number in this limit. At this point, these Reynolds number independent similarity solutions are entered into the equations of motion for the outer flow. After using the chain rule and rearranging the terms in the outer boundary layer equation, a transformed similarity equation is obtained. The thought behind this equation is that the different terms must remain in relative balance between each other, thus yielding the equilibrium similarity conditions between the scales. Consequently,

$$\delta\frac{dU_\infty}{dx}\sim\frac{\delta U_\infty}{U_{\rm so}}\frac{dU_{\rm so}}{dx}\sim\delta\frac{dU_{\rm so}}{dx}\sim U_\infty\frac{d\delta}{dx}\sim U_{\rm so}\frac{d\delta}{dx}\sim-\frac{1}{\rho}\frac{dP_\infty}{dx}$$
$$\sim\frac{R_{{\rm so}_{uv}}}{U_{\rm so}}\sim\frac{R_{{\rm so}_u}}{U_{\rm so}}\frac{d\delta}{dx}\sim\frac{R_{{\rm so}_v}}{U_{\rm so}}\frac{d\delta}{dx}$$

The symbol $\sim$ represents the proportionality between each one of the terms (i.e., depending on the streamwise direction). Therefore after applying the similarity analysis to the governing equations of motion (i.e., continuity and boundary layer equations in outer variables), the scales for the dependent variables are given as

$$U_{\rm so}\sim U_\infty \tag{6}$$

$$R_{{\rm so}_{uv}}\sim U_{\rm so}^2\frac{d\delta}{dx}\sim U_\infty^2\frac{d\delta}{dx} \tag{7}$$

$$R_{{\rm so}_u}\sim R_{{\rm so}_v}\sim U_\infty^2 \tag{8}$$

More important, these results are exact only in the limit as $\delta^+\to\infty$. Therefore, the flow may show a dependence on the Reynolds number when this number is finite [21].

Additionally, the pressure parameter denoted as $\Lambda$ is one that must be a constant in order for an equilibrium pressure gradient flow to exist and is obtained from the similarity analysis as

$$\Lambda\equiv-\frac{\delta}{U_\infty d\delta/dx}\frac{dU_\infty}{dx}\equiv\frac{\delta}{\rho U_\infty^2 d\delta/dx}\frac{dP_\infty}{dx}=\text{ constant} \tag{9}$$

This equation may suitably be integrated for nonzero values of $\Lambda$; thus giving

$$\delta\sim U_\infty^{-1/\Lambda} \tag{10}$$

for equilibrium flows. It will be shown that this parameter can give further insight on the development of pressure gradient flows.

### B. Self-Similarity and Self-Preservation

As mentioned in the preceding section, the scalings found through means of similarity analysis proposed by Castillo and George [21] have, in the past, provided solutions that are self-similar if the upstream conditions are fixed [7]. Moreover, these particular solutions are ones which collapse to a single curve for a given set of upstream conditions, which come into the problem as boundary conditions. Consequently, the profiles collapse, but to different curves depending on the upstream conditions. However, self-preserving solutions represent the true asymptotic solutions of Townsend [18]. These solutions are also more compelling because they collapse the data into a single curve regardless of the upstream conditions, strength of pressure gradient, and Reynolds number range. Consequently, they represent the true asymptotic profile for a given flow.

Following this definition of a self-preserving solution, Zagarola and Smits [24] proposed a scaling by empirical means

$$\frac{U_\infty-U}{U_\infty(\delta_*/\delta)}=f_{\rm op}(\bar{y},\Lambda) \tag{11}$$

which was later shown theoretically by Castillo [25]. This scaling successfully removes the effects of upstream conditions on the turbulent boundary layers.

The parameter $\delta_*/\delta$ possesses the effects of upstream conditions and local Reynolds number [26–29]. A more specific derivation can be found in Castillo [25] or in Wosnik [30] for ZPG flows. With these mentioned scalings [noted in Eqs. (6–8)], it is possible to analyze the data acquired as well as the benchmark data obtained by Ludwieg and Tillmann [13]. Therefore, the effects of the upstream conditions on the velocity deficit profiles will be investigated using the Castillo and George [21] scaling as well as the Zagarola and Smits [24] scaling. Subsequently, it will be determined if these scalings yield self-similar or self-preserving solutions. Brzek [31] attempted to use this scaling on the Reynolds stresses for the outer flow. An improvement was observed but the collapse is not as drastic as in the mean velocity deficit profiles.

## II. Experimental Setup and Upstream Conditions

The low Reynolds number experiments are designed to investigate the effects of the upstream conditions on the downstream flow. In these experiments, the Reynolds numbers based on momentum thickness ranges from 600 up to 1890 and the near-wall measurements are reported as close as $y^+\approx 2.5$. The external conditions explored are the upstream wind-tunnel speed $U_o$, the size of tripwire $d_o$, the position of the tripwire $x_o$, and the angle of the smooth plate $\alpha$, which changes the strength of the external pressure gradient. These are represented in Table 1 for each of the experiments. In Table 1, these conditions are also expressed in the form of an upstream Reynolds number (i.e., the Reynolds numbers based on the tripwire diameter and the tripwire position, respectively). Also, the Reynolds number range based on the momentum thickness is shown in this table. Furthermore, the ratio between the tripwire size and location could also be used as an upstream condition (i.e., $x_o/d_o$).

### A. Facility

The experiment is performed in the wind-tunnel L2 facility in the department of applied mechanics at Chalmers University of Technology. The wind-tunnel is a conventional closed-loop design, equipped with turning vanes in all four corners, honeycombs, and screens, and has a contraction ratio of 5.6:1 moving into the test section. The test section of the tunnel is 3-m-long, 1.8-m-wide, and 1.25-m-high, where the corners have fillets which decrease in size in the downstream direction. This is done to compensate for the boundary layer developed on the wind-tunnel walls. The freestream turbulence level of this facility is about 0.1%. The glass windows along the test section, as well as top and bottom surfaces, are removed to prevent distortions of the optics used for measuring.

**Table 1 Upstream conditions of the present experiment**

| Case # | $U_o$, m/s | $d_o$, mm | $x_o$, mm | $\alpha$, deg | $Re_{d_o}\times 10^{-2}$ | $Re_{x_o}\times 10^{-4}$ | $Re_\theta$ |
|---|---|---|---|---|---|---|---|
| 1 | 8.6 | 2 | 150 | 3.5 | 11.5 | 8.6 | 1330–2121 |
| 2 | 4.8 | 2 | 150 | 3.5 | 6.3 | 4.8 | 687–1183 |
| 3 | 8.6 | 2 | 300 | 3.5 | 11.4 | 17.2 | 1356–2151 |
| 4 | 8.1 | 2 | 150 | 7.0 | 10.8 | 8.1 | 1080–1759 |

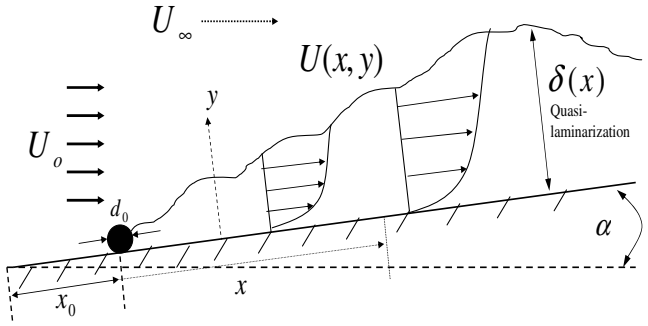


**Fig. 1 Depiction of a turbulent boundary layer subject to a favorable pressure gradient.**

The flow is created using a specially manufactured aluminum plate placed vertically, 200 mm downstream from the start position in the center of the test section. The trailing edge is then rotated to obtain the desired angle $\alpha$, which produces the external favorable pressure gradient. The flat plate has dimensions of 2.5-m-long, 1.25-m-wide, and 5-mm-thick. The nose of the plate is designed to avoid separation in the leading edge of the test section. Additional details are described in Castillo and Johansson [7]. To create a turbulent boundary layer, the boundary layer is tripped using a cylindrical tripwire with a diameter $d_o$, which is positioned across the plate at a distance of $x_o$ from the leading edge of the plate as seen in Fig. 1.

### B. Measuring Probes and Spatial Resolution

The measurements are carried out using laser-doppler anemometry. An argon-ion laser is used as the light source. The laser beam is then separated into four beams of green and blue light to measure the 2-D velocity field. The nearly vertical LDA probe is placed at the top of the wind-tunnel. To reach the desired probe volume and have the probe remain outside of the test section, two beam expanders with an expansion ratio of 1.94:1 are used. The focusing beam expander has an expansion ratio of 1.55:1 and a focal length of 1200 mm. Consequently, the measuring control volume has a diameter of 58 $\mu$m and a length of about 600 $\mu$m. Table 2 shows the size of the smallest turbulent scales $l^*$ (i.e. viscous length scales), the diameter $d$, and the length $l$ of the measuring control volume for the wind-tunnel speeds of approximately 4 and 8 m/s. The data processing of the scattered light collected is carried out using two Dantec BSA processors that rely on the Burstware 3.22 program.

The probe is mounted on a frame made out of aluminum, which is connected to a traverse table. This allows movement of the probe in the streamwise and the wall-normal directions, respectively. The traverse distance in the streamwise direction is from 1.05 to 2.25 m measured from the leading edge of the plate and approximately 60 mm in the normal direction from the surface of the plate.

The measurements closest to the wall are prone to spatial resolution problems (i.e., particularly at wind-tunnel speed of 8.6 m/s where $l^* < d$) mainly due to high velocity gradients at the wall [32]. However, it is possible to achieve measurements as close as $y^+ \sim 2.5$ at a wind-tunnel speed of 4 m/s within 1% accuracy for the turbulence fluctuations with the present configuration and the mean flow is less than 1%. To measure as close to the wall as possible, it is important to determine the distance between the wall and the control volume. This is possible by moving the control volume down to the position of the wall where the light scatter is maximum. This vertical position can be determined within an accuracy of 10 $\mu$m and is repeated for each traverse location.

To bring the probe as close to the wall as possible, the beam closest to the wall must be nearly parallel to it. The flow direction measured is thus making a small angle $\phi$ to the normal of the wall. Consequently, the normal velocity component is then measured in a direction slightly off to the side. In turn, this component is also sensitive to the transverse velocity component. The beam angles are measured within 1%. Because of the small value of the angle $\phi$ ($\phi \leq 1.06$ deg), the values of $\langle v^2 \rangle$ and $\langle uv \rangle$ could be well corrected. This is based on the assumption that the flowfield was homogeneous in the transverse direction (z-direction).

An undesirable effect is the possible influence on the measured normal velocity component by the main stream velocity. This happens if the plane of the two beams used for the measurement of the wall-normal component is tilted slightly in the main stream direction. This problem is prevented by performing test measurements close to the wall ($y^+ \approx 2.5$). At the wall, the fulfillment of the boundary conditions forces the vertical velocity component to be zero. This is achieved by turning the probe around its axis until the detection of a zero mean velocity on the wall-normal direction was obtained. This technique ensures the independency of the signals from each other [7].

**Table 2 Measuring control volume vs viscous length scale for various wind-tunnel speeds**

| Upstream wind-tunnel speed | $U_o$, m/s | 4.8 | 8.6 |
|---|---|---|---|
| Viscous length scales | $l^*$, $\mu$m | 70 | 38 |
| Diameter of control volume | $d$, $\mu$m | 58 | 58 |
| Length of control volume | $l$, $\mu$m | 600 | 600 |

## III. Results

In this favorable pressure gradient experiment, the freestream velocity increases from 8.12 m/s at $x = 1.05$ m up to 9.27 m/s at $x = 2.25$ m with a fixed upstream velocity of 8.6 m/s. For the lower upstream wind-tunnel speed of 4.8 m/s, the freestream velocity outside the boundary layer ranges between 4.76 to 5.00 m/s over the same $x$-interval.

To compare with other experimental data and create a more powerful argument based on the upstream conditions effects and external pressure gradient, the data from Castillo and Johansson [7] for a zero pressure gradient is also used. The data from two different sets of upstream wind-tunnel speeds have been included: one at 5 m/s and another at 10 m/s. The tripwire shape is cylindrical and the diameter of the tripwire is the same for both experiments. Several Reynolds numbers are included based on the tripwire diameter, the tripwire position, and momentum thickness. These quantities are tabulated in Table 3 along with the upstream conditions for the Castillo and Johansson experiment. The same conditions selected by Castillo and Johansson for a ZPG turbulent boundary layer are used here to perform a better comparison.

### A. Velocity Deficit Profiles

Figure 2a shows the mean velocity deficit profiles in a linear–linear scale normalized with the scaling proposed by Castillo and George [21]. This scaling is defined by the freestream velocity as obtained from the equilibrium similarity and the wall-normal coordinate $y$ is normalized by the boundary layer thickness $\delta_{95}$. The data of Ludwieg and Tillmann [13] are included for comparison purposes. Although there are different Reynolds numbers, strengths of pressure gradient, and upstream conditions, the profiles are quite similar. A small difference between the Ludwieg and Tillmann and the present measurements exists. Furthermore, the profiles collapse to a single curve (in Fig. 2b) when using the scaling proposed by Zagarola and Smits [24], $U_\infty \delta_* / \delta$. This proves that the effects of the upstream conditions may not be recognizable on the outer velocity profiles with either scaling.

**Table 3 Upstream conditions of the Castillo and Johansson experiment [7]**

| $U_o$, m/s | $d_o$, mm | $x_o$, mm | $Re_{d_o} \times 10^{-2}$ | $Re_{x_o} \times 10^{-4}$ | $Re_\theta$ |
|---|---|---|---|---|---|
| 10 | 2 | 150 | 13.3 | 10 | 1497–2878 |
| 5 | 2 | 150 | 6.67 | 5 | 737–1571 |

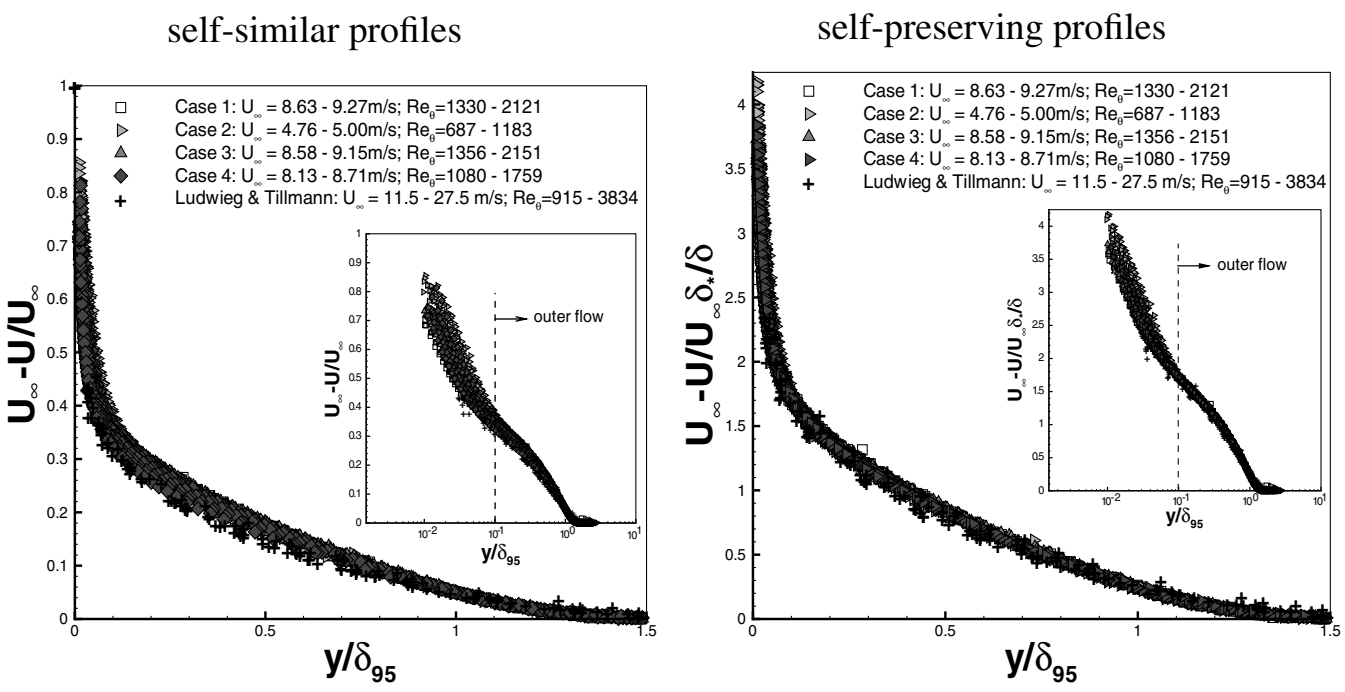


**a) Castillo/George scaling** **b) Zagarola/Smits scaling**

**Fig. 2 Mean velocity deficit profiles normalized by different outer scalings for FPG data.**

Moreover, the Zagarola and Smits [24] scaling yields self-preserving solutions for these flows, even though a small difference in the shape of the profiles might have been anticipated due to the varying external pressure gradient. It is important to note that this conclusion is for the data considered here because Castillo and Walker [33] found three curves: one for each type of pressure gradient flow (i.e., one for ZPG, another for APG, and third for FPG). Therefore, they were able to show that the pressure gradient affects the shape of the velocity deficit profiles.

In Fig. 3, the ZPG data from Castillo and Johansson [7] are added. Figure 3a shows the mean deficit velocity profiles normalized using the freestream velocity. There is a clear influence in the outer flow due to the external pressure gradient imposed by the angle $\alpha$. As the strength of the pressure gradient increases, the profiles tend to move closer to the wall, thus showing the effects of the pressure gradient. In the same manner, it is expected that the skin friction coefficient will increase due to the external favorable pressure gradient. Furthermore, Fig. 3b shows the profiles now normalized by the Zagarola and Smits [24] scaling. This scaling clearly removes the effects of the pressure gradient as well as the upstream conditions for the ZPG and FPG data considered. To isolate the Reynolds number effects from the upstream conditions and the strength of the pressure gradient on the outer flow, the mean velocity deficit profiles are studied at a fixed Reynolds number. In the following paragraph, the results for fixed Reynolds number are considered.

The Reynolds number based on momentum thickness is chosen to be approximately 1750 for various cases of upstream conditions. Consequently, the effects of Reynolds number and pressure gradient

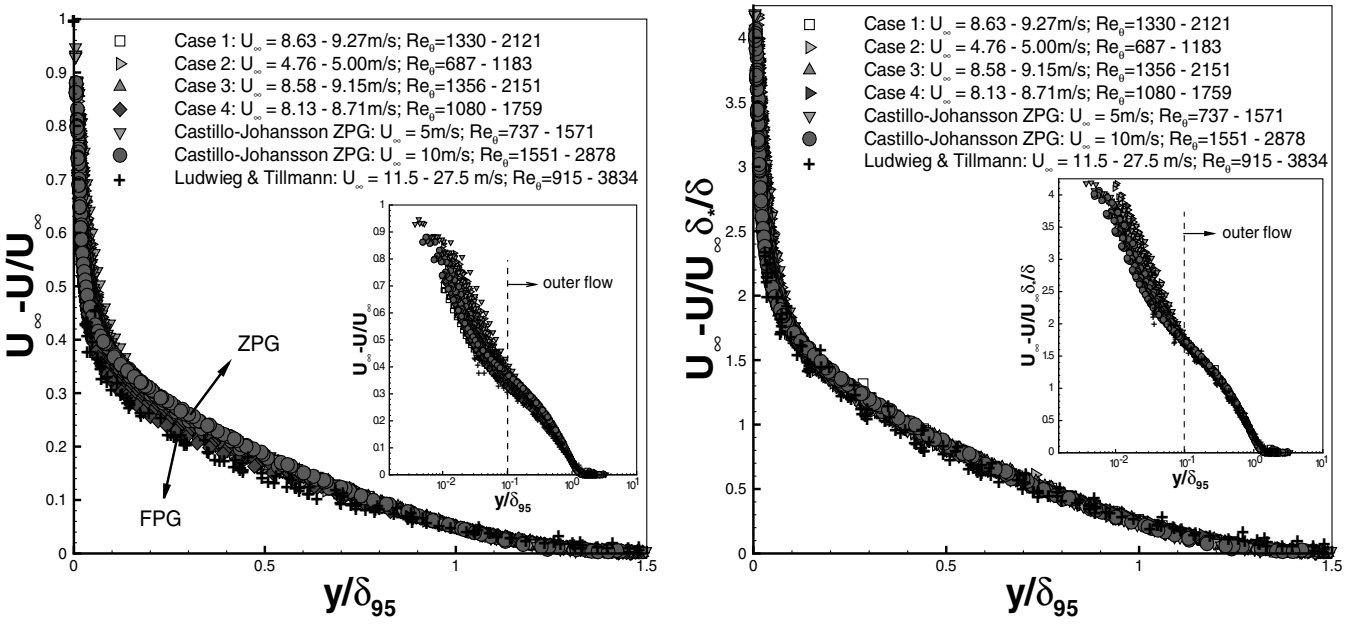


**a) Castillo/George scaling** **b) Zagarola/Smits scaling**

**Fig. 3 Mean velocity deficit profiles normalized by different outer scalings for ZPG/FPG data.**

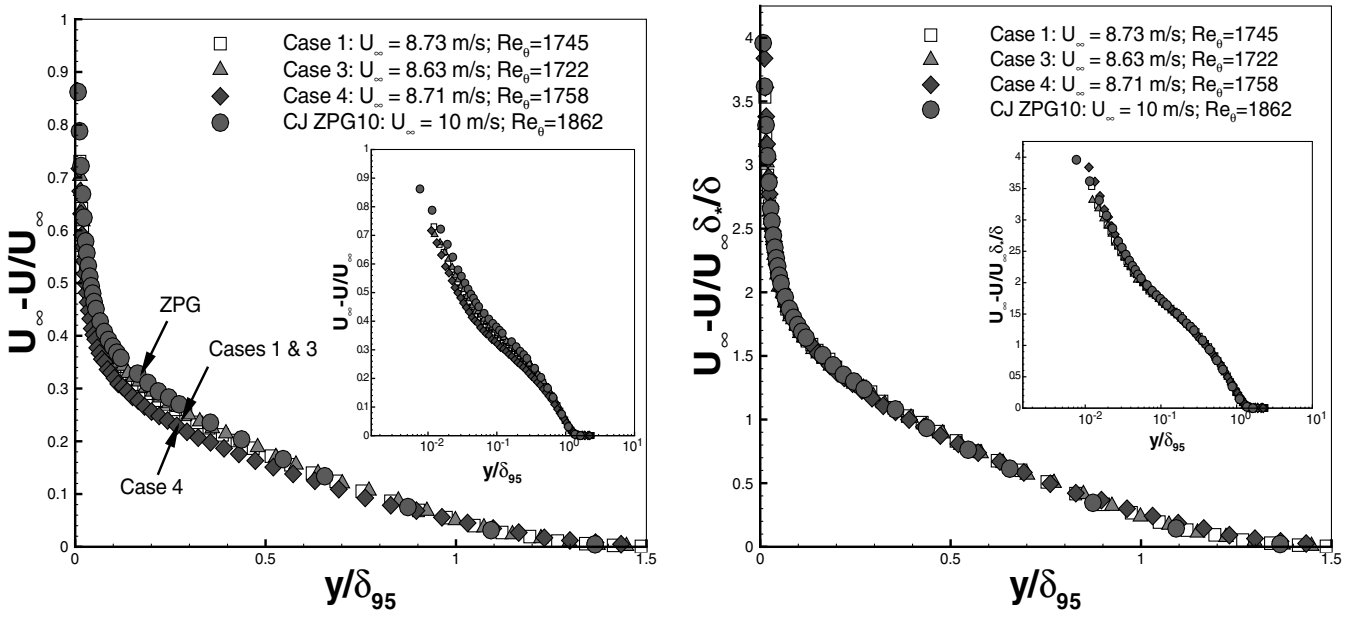


**a) Castillo/George scaling** **b) Zagarola/Smits scaling**

**Fig. 4 Mean velocity profiles normalized with various scalings for fixed Reynolds number, $Re_\theta \approx 1750$.**

are separated. Figure 4 shows the mean velocity deficit profiles normalized using the freestream velocity $U_\infty$ (left), and the Zagarola and Smits [24] scaling $U_\infty(\delta_*/\delta)$ (right). The included upstream condition effects due to the tripwire location are compared between cases 1 and 3. A comparison between cases 1 and 4 depicts the effects caused by the strength of the pressure gradient. The ZPG data of Castillo and Johansson [7] at 10 m/s are also included. These sets of data possess the same tripwire size and location, as well as the same $Re_\theta$. Notice that for a constant Reynolds number of $Re_\theta \approx 1750$, the mean deficit velocity profiles shown in Fig. 4a display a difference due to the strength of the pressure gradient (FPG cases 1, 4, and ZPG). The effect of tripwire location is indistinguishable as seen when comparing cases 1 and 3. The outer flow is clearly sensitive to a relatively strong favorable pressure gradient. However, the Zagarola and Smits [24] scaling is able to capture the effects of the pressure gradient, the local Reynolds number, and the upstream conditions. Therefore, the data in figure Fig. 4b collapse into one single profile.

### B. Reynolds Stress Profiles

The FPG flows studied here as well as the ZPG data of Castillo and Johansson [7] are demonstrated in Fig. 5, where the Reynolds stresses are plotted in outer variables. The scalings are those obtained from the similarity analysis, where the normal stresses are scaled using $U_\infty^2$ and the Reynolds shear stress is normalized using the freestream velocity and the growth rate of the boundary layer, $U_\infty^2(d\delta/dx)$. The Reynolds stresses from Ludwieg and Tillmann [13] are not included because these quantities were not reported by the original authors. As mentioned earlier, the error in the Reynolds stresses is about 1%.

#### 1. *Reynolds Normal Stress Component* $\langle u^2 \rangle$

Figure 5a shows the measured Reynolds stress component normalized with the freestream velocity. High peaks of turbulence occur close to the wall for the streamwise component of the Reynolds stress. These profiles almost fall on top of each other, particularly in the outer region, although a weak dependence on the Reynolds number is observed. When just considering the Reynolds stress data for the streamwise component (including all of the traverses) for all of the different cases, the effect of the upstream wind-tunnel speed produced the largest effect in comparison with the other external conditions (e.g., strength of pressure gradient and position of tripwire).

There is a shift in the peak where the value of the normal stress $\langle u^2 \rangle$ is maximum for the FPG and ZPG profiles. In the profiles, the peak tends to move away from the wall as the strength of the imposed favorable pressure gradient increases. More specifically, the maximum for the ZPG profiles occurs at about $\bar{y} \approx 0.023$, however, for the FPG profiles the maximum is located at $\bar{y} \approx 0.039$.

#### 2. *Reynolds Normal Stress Component* $\langle v^2 \rangle$

Figure 5b shows the Reynolds stress profiles in the wall-normal direction normalized using the freestream velocity $U_\infty^2$. The effects of tripwire are masked when analyzing the data as a whole, but following this section, a meticulous analysis will be performed showing the contrary. Observe that the Reynolds normal stress $\langle v^2 \rangle$ increases as the upstream velocity is decreased. A major difference between various profiles occurs mainly in the mesolayer region between $75 \leq y^+ \leq 375$. As in the $\langle u^2 \rangle$ component of the Reynolds stress, the peak of maximum value shifts towards the right when comparing the ZPG and the FPG profiles. The profiles shift in $\bar{y}$ from about 0.12 to about 0.21 for the ZPG and FPG profiles, respectively. This normalization applies for $\bar{y} > 0.1$ (i.e., the outer flow). More interestingly, this component does not exhibit a significant difference due to the Reynolds number, but mostly due to the changes in pressure gradient strength.

#### 3. *Reynolds Shear Stress Component* $-\langle uv \rangle$

In Figs. 5c and 5d, the Reynolds shear stress component $-\langle uv \rangle$ is normalized with both the freestream velocity $U_\infty^2$ and the scaling obtained from similarity analysis $U_\infty^2(d\delta/dx)$. It is noticeable that this component does not collapse to a single curve and the effect of the upstream conditions are visible when using the freestream velocity $U_\infty$, as seen in Fig. 5c. An even more radical difference occurs when scaling the Reynolds shear stress with $U_\infty^2(d\delta/dx)$ as observed in Fig. 5d. A clear difference between the ZPG and FPG flows is visible with the latter scaling. The ZPG profiles fall much lower than the FPG experiments due to the different growth rates (i.e., $d\delta/dx$) and the case with the highest pressure gradient (case 4) falls above the other cases. Moreover, there is a slight local Reynolds number variation on the flow, which is larger on the FPG data. The effects of the tripping condition are indistinguishable when comparing cases 1 and 3. The lower velocity produces an increase in Reynolds shear stress. Moreover, the Reynolds shear stress $-\langle uv \rangle$ is

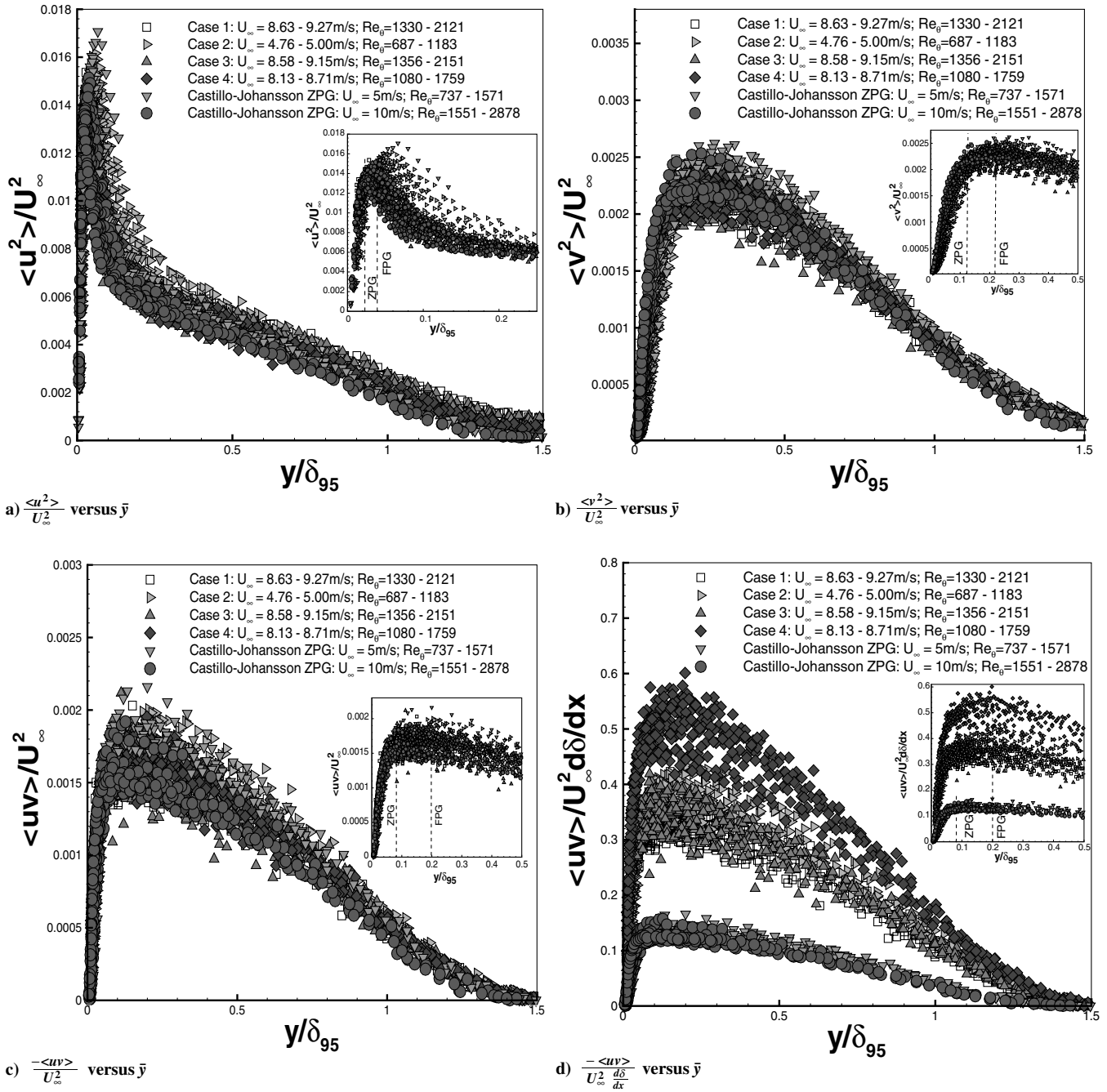


a) $\frac{\langle u^2\rangle}{U_\infty^2}$ versus $\bar{y}$

b) $\frac{\langle v^2\rangle}{U_\infty^2}$ versus $\bar{y}$

c) $\frac{-\langle uv\rangle}{U_\infty^2}$ versus $\bar{y}$

d) $\frac{-\langle uv\rangle}{U_\infty^2 \frac{d\delta}{dx}}$ versus $\bar{y}$

**Fig. 5 Reynolds stresses subject to FPG and ZPG.**

influenced by the upstream conditions because it depends not only on the local parameters of the turbulent boundary layer, but it also depends on the streamwise gradient of these local parameters as found by Perry et al. [34]. There is a shift in the maximum value for the Reynolds shear stress when normalized with both scalings. The maximum values for the profiles tend to move away from the wall as the strength of the external FPG increases. The shift in the normalized wall-normal similarity coordinate $\bar{y}$ is the same amount in Figs. 5c and 5d. The maximum peak shifts from 0.08 to about 0.20 for the ZPG and FPG, respectively.

### 4. *Reynolds Stress Profiles at Fixed Reynolds Number*

Figure 6 displays a more selected set of data where the local Reynolds number is kept approximately constant ($Re_\theta \approx 1700$). In Fig. 6a, it is observed that the data points for case 1 lay above the other experimental data points. Slightly below, but clearly distinguishable from these points, are the data points from case 3. These data points differ from those of case 1 only in the position of the tripwire and it can be concluded that there is indeed an effect on the $\langle u^2\rangle$ component by the tripping conditions, although this effect is quite small.

For example, the data points for the different pressure gradients come in an irregular order. The data for the ZPG fall in between the data points for the weak FPG case (case 1) and the stronger FPG case (case 4), which is further indication that the profiles are affected by the tripping condition. This is mainly due to the effect of the upstream wind-tunnel speed, which indeed affects the Reynolds numbers and is a way of controlling the upstream conditions given that $Re_{x_o} = (U_o x_o)/\nu$. It can also change the shape of the profiles as seen previously. In addition, there is a clear effect on the $\langle u^2\rangle$ component due to the strength of the external pressure gradient. Note that the upstream conditions for cases 1 and 4 are identical (for the same $Re_\theta$) except for the pressure gradient.

In Fig. 6b, the effects of pressure gradient and tripwire position on $\langle v^2\rangle$ are observed. Here, the cases 1 and 3 together with the ZPG case

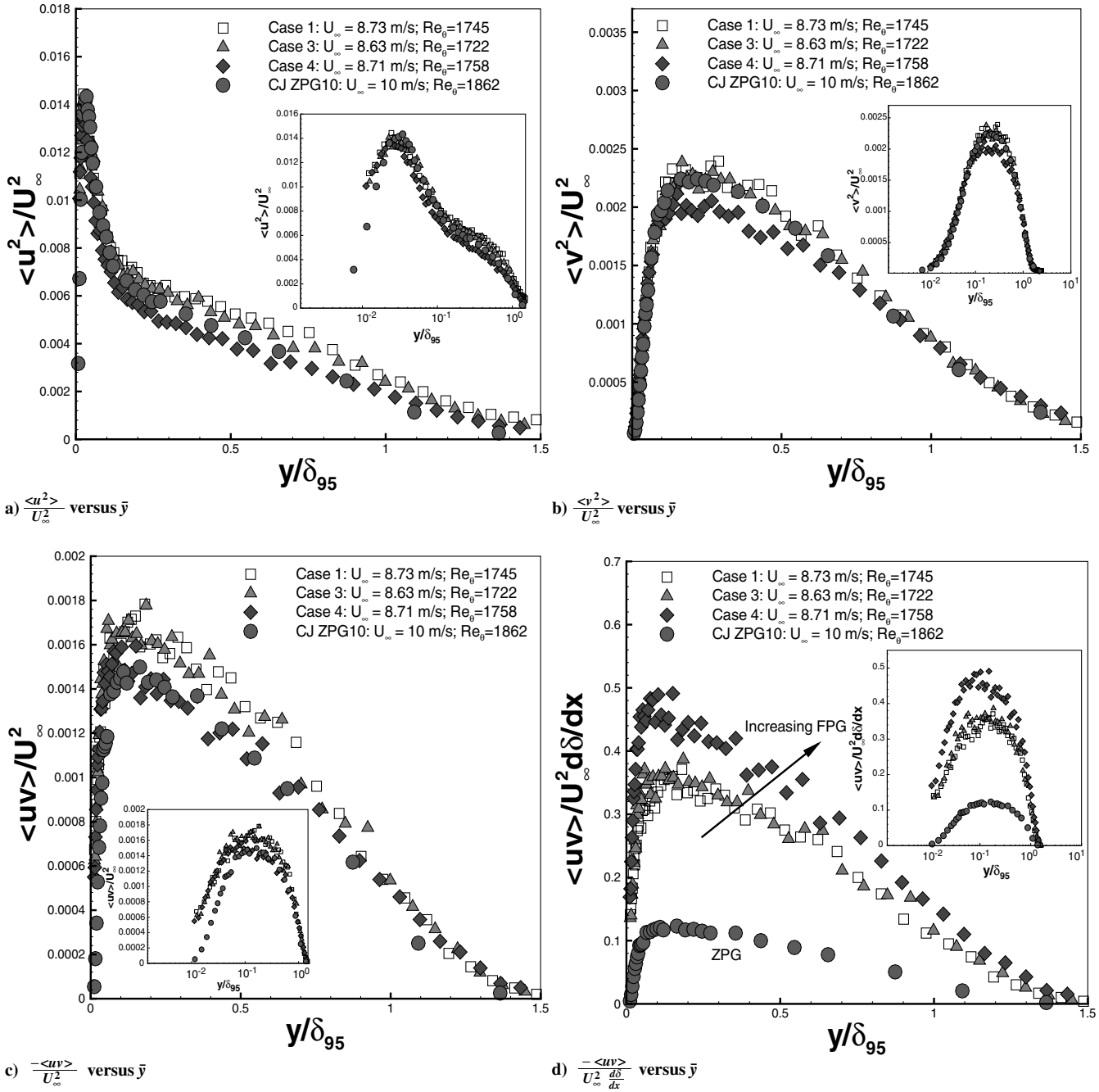


**a)** $\frac{\langle u^2\rangle}{U_\infty^2}$ **versus** $\bar{y}$ **b)** $\frac{\langle v^2\rangle}{U_\infty^2}$ **versus** $\bar{y}$

**c)** $\frac{-\langle uv\rangle}{U_\infty^2}$ **versus** $\bar{y}$ **d)** $\frac{-\langle uv\rangle}{U_\infty^2 \frac{d\delta}{dx}}$ **versus** $\bar{y}$

**Fig. 6 Reynolds stresses subject to FPG and ZPG for fixed Reynolds number, $Re_\theta \approx 1750$.**

fall into one group (within the scatter of the data). On the other hand, case 4, the stronger pressure gradient, falls below the other data points. Clearly, there is an effect of the pressure gradient on $\langle v^2\rangle$, but the data do not support that there should be an effect due to the change in tripwire location. It is worth noting that Johansson and Castillo [23] found the opposite trend with regard to the effect of tripping conditions. They did not observe any effect on $\langle u^2\rangle$ due to the tripwire location, however, a clear effect on the $\langle v^2\rangle$ component was seen for ZPG flows. The reason for this discrepancy is presently not known.

In Figs. 6c and 6d, the effect of pressure gradient and tripwire location are shown on the Reynolds shear stress $\langle uv\rangle$. Figure 6c shows a clear effect of the pressure gradient (comparing cases 1 and 4, which differ only in the strength of the pressure gradient). The data points for the ZPG case fall close to those of case 4, which again is somewhat surprising because one would have expected to observe a consecutive series in the data for the three different pressure gradients. However, notice that the ZPG profile has a wind-tunnel speed of 10 m/s which is higher than that of the FPG profiles. This may be the reason for the departure from cases 1 and 3. The data points of cases 1 and 3 (which differ in tripwire position only) practically fall on top of each other within the scatter of the data. No conclusion can be made for the $\langle uv\rangle$ component in terms of the tripwire position. The scatter in the data is, however, significant and the possibility that more accurate measurements might reveal such effect cannot be excluded.

Moreover, the ZPG measurements of Castillo and Johannson [7] showed an effect of the upstream conditions on the Reynolds shear stress. The fact that the ZPG case produces data points close to those of case 4 (stronger FPG) may indicate a possible dependence on the upstream conditions due to the upstream wind-tunnel speed. In Fig. 6d, the effect of the pressure gradient is again clearly

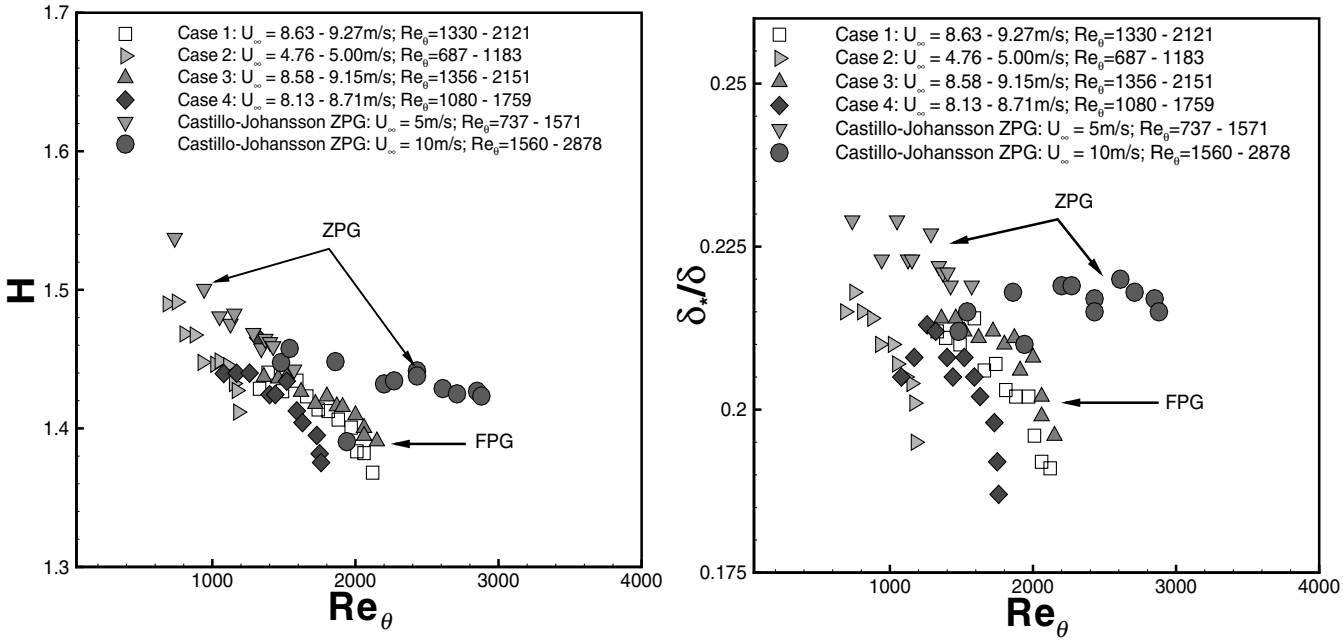


**a) Shape factor versus $Re_\theta$** **b) $\frac{\delta_*}{\delta}$ versus $Re_\theta$**

**Fig. 7 Boundary layer parameters.**

demonstrated when scaling the Reynolds shear stress using the Castillo and George [21] scaling which includes the growth of the boundary layer $d\delta/dx$ and the freestream velocity $U_\infty$. Still (compare cases 1 and 3), the effect from the tripwire location cannot be detected.

### C. Boundary Layer Parameters

Flow parameters such as shape factor, displacement thickness, and boundary layer growth are investigated in this section. In Fig. 7a, the shape factor $H$ vs Reynolds number $Re_\theta$ is shown. For all cases, the shape factor tends to decrease as the Reynolds number increases. Furthermore, the effect of the pressure gradient is evident, although the scatter in the data is quite significant. Also, it can be noticed that all the FPG profiles are below the ZPG values. In addition, there also seems to be an effect due to the tripwire location, although this effect is less evident. A similar behavior exists for the ratio of the displacement thickness and the boundary layer thickness as shown in Fig. 7b. However, this parameter shows a clear difference between different tripwire locations. This is to be expected because this parameter is used in the Zagarola and Smits [24] scaling and this scaling has proven to capture the influence of the Reynolds number and upstream conditions [33] successfully. Also, the decrease in magnitude of both parameters, $H$ and $\delta_*/\delta$, is far more significant in the FPG data than the ZPG data.

### D. Boundary Layer Growth

Figure 8 shows the growth of the boundary layer by plotting $Re_\delta$ vs $Re_x$, where $\delta_{95}$ is the boundary layer thickness and $x$ represents the downstream position. It is observed that the boundary layers grow differently and depend on the upstream conditions and the external pressure gradient. As expected, it is shown that ZPG boundary layers are thicker and grow faster than FPG boundary layers. The boundary layer grows slower as the external pressure gradient is increased and as the upstream wind-tunnel speed is decreased. Cases 1 and 3, which differ only in tripwire location, are indistinguishable, thus indicating that these conditions have a negligible effect on the boundary layer growth. Case 2 differs from case 1 only in the magnitude of the upstream wind-tunnel speed. Yet, for the same Reynolds number, the boundary layers differ slightly. However, it should be noted that the tripwire position for these two cases are different. This clearly indicated that there is some influence on the boundary layer growth by the location of the tripwire condition.

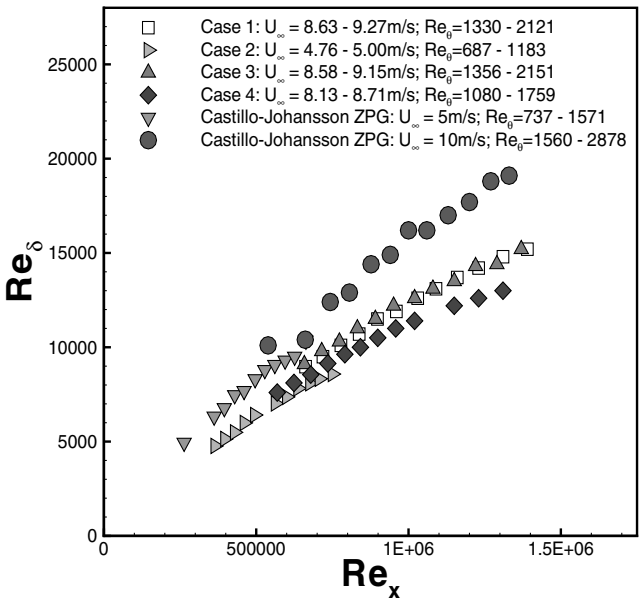


**Fig. 8 Boundary layer growth.**

### E. Pressure Parameter

According to the similarity analysis carried out, a flow is found to be in equilibrium if the pressure parameter $\Lambda$ is a constant

$$\Lambda \equiv -\frac{\delta}{U_\infty d\delta/dx}\frac{dU_\infty}{dx} \equiv \frac{\delta}{\rho U_\infty^2 d\delta/dx}\frac{dP_\infty}{dx}$$

However, the flow in the present experiment is a developing FPG flow or nonequilibrium flow due to the fact that the pressure parameter is not constant. A large number of data points fall on the ZPG line as seen in Fig. 9a. However, the mean deficit velocity and Reynolds stress profiles in this region of ZPG and FPG are nearly

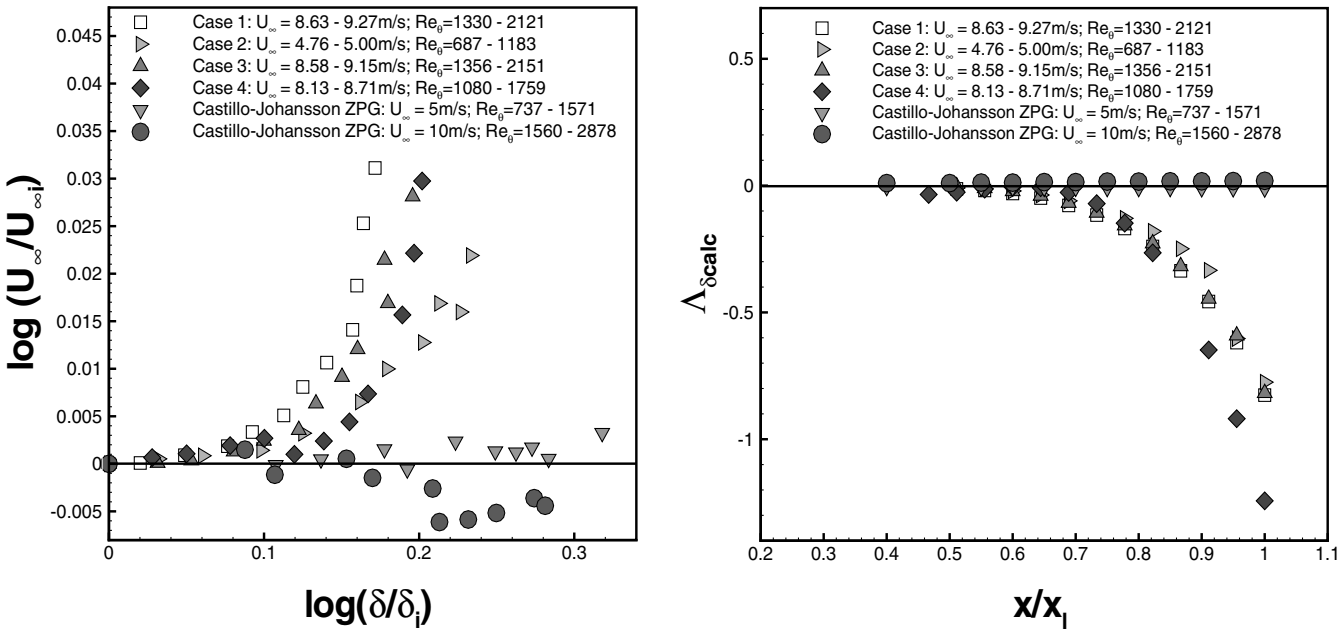


**a)** $log(\frac{U_\infty}{U_{\infty i}})$ **versus** $log(\frac{\delta}{\delta_i})$ **b)** $\Lambda_{\delta calc}$ **versus** $\frac{x}{x_l}$

**Fig. 9 Pressure parameter Λ.**

identical. This leads to the conclusion that these flows are not in global equilibrium. However, fairly close to the leading edge they can be considered to be in local equilibrium. All of these arguments may be observed in Fig. 9a, where $\log(U_\infty/U_{\infty i})$ vs $\log(\delta/\delta_i)$ is plotted. The variables in the denominator $U_{\infty i}$ and $\delta_i$ are the values of the freestream velocity and boundary layer thickness at the first measurement location for the particular data set considered. There is a notable progression of the pressure parameter and for these data. Consequently, there is not an asymptotic value observed within the evaluated Reynolds number range.

The local value is also found through a direct calculation of the pressure parameter by computing directly the growth rate of the boundary layer, $d\delta/dx$ and $dU_\infty/dx$. The value is attained at each particular traverse, because the different quantities in the equation are measured. The progression of the pressure parameter is seen in Fig. 9b. The plot shows the calculated value of the pressure parameter $\Lambda_{\delta\text{calc}}$ vs $x/x_l$, the downstream position normalized using the last measurement position for each position in the experiment. After $x/x_l = 0.6$, the flow begins its development into an FPG flow. Notice that an asymptotic value of the calculated pressure parameter $\Lambda_{\delta\text{calc}}$ for the values of $d\delta/dx$ and $dU_\infty/dx$ is not achieved. Instead, it shows the progression, which again categorizes these flows as nonequilibrium or developing flows (i.e., $\Lambda \neq$ constant). More important, the effect of the pressure gradient is clearly seen in the plot given by case 4, which has a stronger FPG than case 1, thus showing a faster and larger growth of the parameter.

The effects in cases 2 and 3 are less noticeable. It is an unfortunate shortcoming of the present investigation that the plate used was too short to be able to demonstrate whether or not the pressure parameter would eventually reach an asymptotic value. The ZPG data from Castillo and Johansson [7] at 10 m/s is also included in this figure. As expected for any ZPG flow, this ZPG turbulent boundary layer should have a pressure parameter of zero or nearly zero.

Observing the results from a larger scope and considering other data from different researchers, the results are quite intriguing. The data sets are taken from a wide variety of sources and flow conditions including all types of pressure gradients (zero, favorable, and adverse) [8,9,13–17,31,34–39]. In Fig. 10, the data is normalized by $U_{\infty i}$ and $\delta_i$ as done previously in Fig. 9, where the logarithmic quantities of the normalized freestream velocity and boundary layer thickness are used. Remarkably, the four different types of flows, ZPG, APG, FPG, and quasi-laminar, are found to be associated with three different quadrants.

Figure 10 shows all the quadrants where quadrant 1 is a region for turbulent FPG flows. Quadrant 2 describes flows that are in a quasi-laminar state or flows approaching this state, thus indicating that the boundary layer thickness decreases as the flow develops downstream. This state is recognized in this manner given that the boundary layer never reaches a true laminar state because it contains residual effects due to the Reynolds stresses, hence the term quasi-laminar. The quasi-laminar region changes all the way to 0.47 for the data considered here. A third quadrant, denoted by quadrant 4, includes all turbulent adverse pressure gradient flows. The line dividing the turbulent FPG and APG flows is a line which describes the zero pressure gradient flows. Developing flows may fall into different quadrants, such as the data of Jones et al. [17] as well as the data of Schubauer and Klebanoff [35].

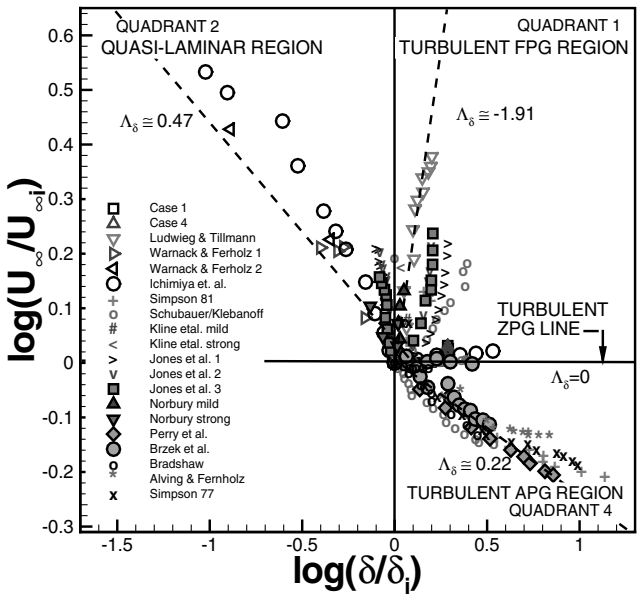


**Fig. 10 Plot of** $\log(U_\infty/U_{\infty i})$ **vs** $\log(\delta/\delta_i)$**.**

Previously, Castillo and George [21] found a pressure parameter value for equilibrium FPG turbulent flows of $\Lambda \cong -1.92$ for most of the data available at that time. It is clear that it is easier to obtain a wider range of values for an FPG flow than for an APG flow. This supports the argument that it is easier for the data to fall in the previous value of about 0.22 as seen in quadrant 4. Figure 10 also allows the categorization of turbulent FPG flows, quadrant 1, quasi-laminar flows, quadrant 2, and turbulent APG flows, quadrant 4.

Castillo and George [21] suggested a single value for each type of pressure gradient for the considered data (e.g., 0 for ZPG, $-1.92$ for FPG, and 0.22 for APG), but according to the data evaluated here, the pressure parameter is not confined to a single value. Moreover, this suggests that for a particular set of experimental conditions (a single experiment), there can be either 1) a single value of the pressure parameter, 2) different values for a nonequilibrium flow (local regions of APG, ZPG, FPG, and/or quasi-laminar), or 3) developing values if the flow shows a progression as seen from the present LDA data.

## IV. Conclusions

This is the first time experiments on favorable pressure gradient turbulent boundary layers are carried out with such detailed information about upstream conditions and multiple traverses acquired using LDA. The main results of the present investigation are summarized, based on the analysis of the acquired LDA experimental data using the scalings proposed by Castillo and George [21] for the mean velocity deficit and Reynolds stresses. The mean deficit profiles subject to FPG and ZPG collapse with the freestream velocity, but the curves are slightly different due to the strength of the external pressure gradient, *thus yielding self-similar solutions which depend on their boundary conditions.* The dependencies of the external pressure gradient, the upstream wind-tunnel speed, and tripwire position are all removed from the mean deficit profiles when normalized by the Zagarola and Smits [24] scaling $U_\infty \delta_*/\delta$; *this scaling yields self-preserving solutions* as sought by Townsend [18] and are independent of the upstream conditions.

For the Reynolds stress profiles, the effects of the upstream conditions can be clearly identified in the outer flow. For all Reynolds stresses, a clear dependence on the pressure gradient is demonstrated and the peaks of the Reynolds stresses changes with the imposed pressure gradient. Moreover, these peaks move from left to right (away from the wall) as the FPG increases. Also, there is a clear dependence on the Reynolds number, particularly for the $\langle u^2 \rangle$ component. Moreover, the Reynolds stresses also show dependencies on the upstream conditions.

The boundary layer parameters (i.e., shape factor and boundary layer growth) are prone to the influence of the upstream conditions. For instance, the shape factor and the ratio $\delta_*/\delta$ tend to decrease as the Reynolds number and the strength of the pressure gradient increase. The boundary layer growth is able to portray the effects of upstream conditions. The boundary layers grow differently depending on the boundary conditions imposed on the flow. Furthermore, it is shown that the boundary layer is not in equilibrium because $\Lambda \neq$ constant.

Furthermore, three quadrants are found describing different types of flows: quadrant 1 (turbulent FPG), quadrant 2 (quasi-laminar), and quadrant 4 (turbulent APG flows). The line $\log(U_\infty/U_{\infty i}) = 0$ ($\Lambda = 0$) for ZPG flows divides the FPG and APG regions. Different values of the pressure parameter are found for a given set of upstream or experimental conditions, contrary to the three unique values found by Castillo and George [21].

## Acknowledgments

Special thanks to Ronald Joslin from Office of Naval Research and Roosevelt Johnson from the National Science Foundation: Alliance for Graduate Education and the Professoriate program for their support in this investigation.

## References

[1] Klebanoff, P. S., and Diehl, Z. W., "Some Features of Artificially Thickened Fully Developed Turbulent Boundary Layers with Zero Pressure Gradient," NACA TM 1110, 1952.

[2] Gad-el-Hak, M., "Flow Control: Passive, Active and Reactive Flow Management," Cambridge Univ. Press, Cambridge, England, U.K., 2000, p. 101.

[3] Clauser, F. H., "Turbulent Boundary Layers in Adverse Pressure Gradients," *Journal of the Aeronautical Sciences*, Vol. 21, No. 2, 1954, pp. 91–108.

[4] von Kármán, T., Mechanische Aehnlichkeit und Turbulenz , Nachr. Ges. Wiss. Göttingen, 68, 1930.

[5] Millikan, C. M., "A Critical Discussion of Turbulent Flows in Channels and Circular Tubes," *Proceedings of the 5th International Congress of Applied Mechanics*, Wiley, New York, 1938, pp. 386–392.

[6] Erm, L. P., and Joubert, P. N., "Low-Reynolds-Number Turbulent Boundary Layers," *Journal of Fluid Mechanics*, Vol. 230, 1991, pp. 1–44.

[7] Castillo, L., and Johansson, T. G., "Effects of the Upstream Conditions on a Low Reynolds Number Turbulent Boundary Layer with Zero Pressure Gradient," *Journal of Turbulence*, Vol. 3, 2002, p. 31.

[8] Warnack, D., and Fernholz, H. H., "Effects of a Favorable Pressure Gradient and of the Reynolds Number on an Incompressible Axissymmetric Turbulent Boundary Layer, Part 2: The Boundary Layer with Relaminarization," *Journal of Fluid Mechanics*, Vol. 359, 1998, pp. 357–381.

[9] Ichimiya, M., Nakamura, I., and Yamashita, S., "Properties of a Relaminarizing Turbulent Boundary Layer Under a Favorable Pressure Gradient," *Experimental Thermal and Fluid Science*, Vol. 17, No. 1, 1998, pp. 37–48.

[10] Escudier, M. P., Abdel-Hameed, A., Johnson, M. W., and Sutcliffe, C. J., "Laminarization and Re-Transition of a Turbulent Boundary Layer Subjected to Favorable Pressure Gradient," *Experiments in Fluids*, Vol. 25, Nos. 5–61998, pp. 491–502.

[11] Launder, B. E., "Laminarization of the Turbulent Boundary Layer in a Severe Acceleration," *Journal of Applied Mechanics*, Vol. 31, 1964, pp. 707–708.

[12] Sreenivasan, K. R., "Laminarescent, Relaminarizing and Retransitional Flows," *Acta Mechanica*, Vol .44, 1982, pp. 1–48.

[13] Ludwieg, H., and Tillmann, W., "Investigations of the Wall Shearing Stress in Turbulent Boundary Layers," NACA TM 1285, 1950.

[14] Herring, H. J., and Norbury, J. F., "Some Experiments on Equilibrium Turbulent Boundary Layers in Favourable Pressure Gradients," *Journal of Fluid Mechanics*, Vol. 27, 1966, pp. 541–549.

[15] Kline, S. J., Reynolds, W. C., Schraub, F. A., and Runstadler, P. W., "Structure of Turbulent Boundary Layers," *Journal of Fluid Mechanics*, Vol. 30, 1967, pp. 741–773.

[16] Fernholz, H. H., and Warnack, D., "Effects of a Favorable Pressure Gradient and of the Reynolds Number on an Incompressible Axissymmetric Turbulent Boundary Layer, Part 1: The Turbulent Boundary Layer," *Journal of Fluid Mechanics*, Vol. 359, 1998, pp. 329–56.

[17] Jones, M. B., Marušić, I., and Perry, A. E., "Evolution and Structure of Sink-Flow Turbulent Boundary Layers," *Journal of Fluid Mechanics*, Vol. 428, 2001, pp. 1–27.

[18] Townsend, A. A., "Equilibrium Layers and Wall Turbulence," *Journal of Fluid Mechanics*, Vol 11, No. 1, 1961, pp. 97–120.

[19] Rotta, J. C., "Turbulent Boundary Layers in Incompressible Flow," *Progress in Aeronautical Sciences*, Vol. 2, 1962, pp. 1–219.

[20] Skåre, P. E., and Krogstad, P., "A Turbulent Equilibrium Boundary Layer Near Separation," *Journal of Fluid Mechanics*, Vol. 272, 1994, pp. 319–348.

[21] Castillo, L., and George, W. K., "Similarity Analysis for Turbulent Boundary Layer with Pressure Gradient: Outer Flow," *AIAA Journal*, Vol. 39, No. 1, 2001, pp. 41–47.

[22] George, W. K., "Some New Ideas for Similarity of Turbulent Shear Flows," *Turbulence, Heat and Mass Transfer 1*, edited by K. Hanjalic and J. C. F. Pereira, Begell House, NY, ISBN 1-56700-040-1, 1994, pp. 13–24.

[23] Johansson, T. G., and Castillo, L., "LDA Measurements in Turbulent Boundary Layers with Zero Pressure Gradient," *In Turbulence and Shear Flow Phenomena*, TSFP-2, Universitetservice AB, Stockholm, 2002.

[24] Zagarola, M. V., and Smits, A. J., "Mean-Flow Scaling of Turbulent Pipe Flow," *Journal of Fluid Mechanics*, Vol. 373, 1998, pp. 33–79.

[25] Castillo, L., Application of Zagarola/Smits Scaling in Turbulent Boundary Layers with Pressure Gradient, edited by M. Rahman, and C.

A. Brebbia, *Advances in Fluid Mechanics 3*, WIT Press, Montreal, Canada, 2000, pp. 275–288.
[26] Wang, X., "Similarity Analysis for Turbulent Boundary Layers Subject to Pressure Gradient and Heat Transfer," Ph.D. Dissertation, Rensselaer Polytechnic Inst., Troy, New York, 2003.
[27] Wang, X., and Castillo, L., "Asymptotic Solutions in Forced Convection Turbulent Boundary Layers," *Journal of Turbulence*, Vol. 4, 2003, p. 6.
[28] Seo, J., "Investigation of the Upstream Conditions and Surface Roughness in Turbulent Boundary Layers," Ph.D. Dissertation, Rensselaer Polytechnic Inst., Troy, New York, 2003.
[29] Cal, R. B., and Castillo, L., 2005, "Similarity Analysis for Transpired Turbulent Boundary Layers Subjected to External Pressure Gradients," *AIAA Journal*, Vol. 43, No. 9, 2005, pp. 1913–1922.
[30] Wosnik, M., "On Wall-Bounded Turbulent Flows," Ph.D. Thesis, State Univ. of New York, Buffalo, NY, 2000.
[31] Brzek, B., "Development and Characterization of an Increasing Adverse Pressure Gradient Turbulent Boundary Layer," M.S. Thesis, Rensselaer Polytechnic Inst., Troy, NY, 2005.
[32] Johansson, T. G., and Karlsson, R. I., "Energy Budget in the Near-Wall Region of a Turbulent Boundary Layer," edited by R. Adrian, D. F. G. Durao, F. Durst, and J. H. Whitelaw, *Applications of Laser Anemometry to Fluid Mechanics*, Springer–Verlag, Berlin, 1989, pp. 3–22.
[33] Castillo, L., and Walker, D., "Effects of the Upstream Conditions on Turbulent Boundary Layers," *AIAA Journal*, Vol. 40, No. 12, 2002, pp. 2540–2542.
[34] Perry, A. E., Marušić, I., and Li, J. D., "Wall Turbulence Closure Based on Classical Similarity Laws and the Attached Eddy Hypothesis," *Physics of Fluids*, Vol. 6, No. 2, 1994, pp. 1024–1035.
[35] Schubauer, G. B., and Klebanoff, P., "Forced Mixing in Boundary Layers," *Journal of Fluid Mechanics*, Vol. 8, 1951, pp. 10–32.
[36] Simpson, R. L., and Chew, Y. T., "Structure of a Separating Turbulent Boundary Layer," *Journal of Fluid Mechanics*, Vol. 113, 1981, pp. 23–51.
[37] Simpson, R. L., and Strickland, J. H., "Features of a Separating Turbulent Boundary Layer in the Vicinity of Separation," *Journal of Fluid Mechanics*, Vol. 79, 1977, pp. 553–594.
[38] Alving, A. E., and Fernholz, H. H., "Turbulence Measurements Around a Mild Separation Bubble and Downstream of Reattachment," *Journal of Fluid Mechanics*, Vol. 322, 1996, pp. 297–328.
[39] Bradshaw, P., "Turbulent Structure of Equilibrium Boundary Layers," *Journal of Fluid Mechanics*, Vol. 29, 1967, pp. 625–645.

A. Tumin
*Associate Editor*